The Effect of Carbon Nanotube Waviness and Aspect Ratio on the Buckling of Cross-Ply Laminated FG-CNTRC Plates Using EFG Method

Sh. Shams
Young Researchers and Elite Club,
Islamic Azad University, Mobarakeh Branch, Mobarakeh, Iran
E-mail: shahrooz.shams@gmail.com

B. Soltani*
Faculty of Mechanical Engineering,
University of Kashan, Kashan, Iran
E-mail: bsoltani@kashanu.ac.ir
*Corresponding author

Received: 6 August 2015, Revised: 15 November 2015, Accepted: 19 December 2015

Abstract: This article deals with the buckling analysis of perfectly bonded cross-ply laminated composite plates reinforced by wavy carbon nanotubes (CNTs) under in-plane loads using element free Galerkin (EFG) method based on first-order shear deformation theory (FSDT). The wavy single-walled CNTs and Poly-co-vinylene are used for the fibers and the matrix, respectively. The CNT fibers are distributed in the polymer matrix in four types of arrangements in each layer. The material properties of the laminated nanocomposite plates are estimated through a micromechanical model based on the extended rule of mixture. The minimum potential energy approach is utilized to obtain the governing equations and the stiffness matrices. Full transformation approach is employed to enforce essential boundary conditions. The accuracy and convergency of the EFG method is established by comparing the obtained results with available literature. Then, the effects of CNT volume fraction and waviness, aspect ratio and distribution type of CNTs as well as plate aspect ratio, plate width-to-thickness ratio and boundary conditions on the buckling behaviour of cross-ply laminated functionally graded carbon nanotube reinforced composite (FG-CNTRC) plates are investigated. The numerical results show that the CNT waviness and aspect ratio have important effects on the buckling behaviour of FG-CNTRC plates.

Keywords: Buckling, Functionally graded materials, Nanocomposite plates

Reference:. Shams. Sh and Soltani .B, 'The Effect of Carbon Nanotube Waviness and Aspect Ratio on the Buckling of Cross-Ply Laminated FG-CNTRC Pates Using EFG Method', Int J of Advanced Design and Manufacturing Technology, Vol. 9/No. 1, 2016, pp. 33–43.

Biographical notes: Sh. Shams is a faculty member in Islamic Azad University, Mobarakeh Branch, Iran. He received his PhD and MSc in Mech. Eng. from Univ. of Kashan, Iran. His research interest includes nanocomposite materials and mesh free methods. **B. Soltani** is Assistant Prof. of Mech. Eng. at Faculty of Mech. Eng. in Univ. of Kashan, Iran. He received his PhD in Mech. Eng. from Chalmers Univ. of Tech., Sweden. His current research focuses on FEM, mesh free method and continuum mechanics.
.

1 INTRODUCTION

Carbon nanotubes (CNTs) have become the most promising reinforcement materials for high performance structural and multifunctional composites, due to its supreme and exceptional mechanical and physical properties since 1990s [1]–[2][3]. Introducing CNTs as reinforcement phase in polymer matrices leaded to several important studies to estimate their mechanical properties accurately [4]–[5]. These studies have proved that applying small amount of CNTs (1% by weight) to the matrix can effectively enhance the thermo-mechanical and electrical properties of nanocomposites [6], [7]. In practice, this behaviour makes them appropriate for aerospace applications as well as electronics and transport industries.

Recently, many investigations considering mechanical response of carbon nanotube reinforced composites (CNTRCs) structures have been done. Jafari Mehrabadi et al. [8] presented mechanical buckling of nanocomposites rectangular plate reinforced by aligned and straight single-walled carbon nanotubes (SWCNTs) based on first-order shear deformation theory (FSDT). They used both the Eshelby-Mori-Tanaka approach and the extended rule of mixture to evaluate the effective material properties of CNTs. Buckling analysis of quadrilateral laminated plates with CNTRC layers employing a mapping-differential quadrature technique is investigated by Malekzadeh and Shojaee [9]. They examined the effects of volume fraction of CNTs, geometrical parameters, thickness-to-length ratio, CNT distribution profiles and boundary conditions on the critical buckling load. Analysis of functionally graded carbon nanotube-reinforced composite (FG-CNTRC) plates was presented by Shen [10] in which he studied the nonlinear bending behaviour of FG-CNTRC plates in thermal environment. He concluded that the load-bending moment curves of the plate could be significantly increased as a result of functionally graded CNT reinforcements.

Zhu et al. investigated linear bending and free vibration behaviours of FG-CNTRC plates with various distributions of reinforcements under different width-to-thickness ratios using finite element method (FEM) [11]. Sobhani Aragh et al. studied the vibration behaviour of continuous graded CNTRC cylindrical panel using an equivalent continuum model based on Eshelby-Mori-Tanaka approach [12]. They demonstrated that continuously graded oriented CNT volume fractions can be used for management of vibration behaviour of structures. Alibeigloo and Liew [13] presented a thermoelastic analysis of FG-CNTRC plates based on three-dimensional theory of elasticity. They investigated the effects of uniform and functionally graded distributions of CNTs, their volume fractions as well as length-to-thickness ratio of the plate. Static analysis of FG-CNTRC cylinders considering an axisymmetric model using element-free Galerkin (EFG) method was presented by Moradi-Dastjerdi et al. [14]. Furthermore, Moradi-Dastjerdi et al. investigated the effects of CNT waviness on the dynamic behavior of FG-CNTRC cylinder under impact load. They concluded that waviness has a significant effect on the dynamic behaviour of the nanocomposite cylinder [15]. Large deflection analysis of FG-CNTRC plates by element-free *kp*-Ritz method based on von Kármán assumption was studied by Lei et al. [16]. The obtained results revealed that the change of CNT contents, plate width-to-thickness ratio and boundary conditions have pronounced effects on nonlinear responses of different types of CNTRC plates.

Furthermore, buckling analysis of FG-CNTRC plates using element-free *kp*-Ritz method was presented by Lei et al. [17]. They concluded that the distribution type of CNT significantly affects buckling strength of CNTRC plates. Nonlinear vibration of shear deformable CNTRC cylindrical panels resting on elastic foundations in thermal environments was studied by Shen and Xiang [18]. They revealed that the natural frequencies are increased by increasing the CNT volume fraction, while the CNTRC panels with intermediate CNT volume fraction do not necessarily have intermediate nonlinear to linear frequency ratios. Shen investigated thermal buckling and postbuckling behaviour of laminated CNTRC plates subjected to in-plane temperature variation and resting on elastic foundation based on higher order shear deformation theory [19]. He concluded that the influence of functionally graded arrangement of CNTs on the buckling and postbuckling behavior of FG-CNTRC plates is more pronounced in comparison with plates with metal matrix.

Elastic buckling of circular and annular plates reinforced with CNTs is investigated by Jam et al. [20] using optimized Rayleigh-Ritz method. The effects of CNTs orientation angle, boundary conditions, geometric ratio of plate and agglomeration of CNTs were carried out. Free vibration characteristics of nanocomposite cylindrical panels reinforced by single-walled CNTs were presented by Jam et al. [21] using generalized differential quadrature method. They showed that distribution species and volume fractions of CNTs have significant effects on normalized natural frequency. The buckling analysis of annular composite plates reinforced by CNTs under compressive and torsional loads was investigated by Asadi and Jam. They used analytical method and FEM to study the effects of CNT volume fractions, orientation angles, boundary conditions and geometric ratio of plates [22].

Kamarian et al. used Eshelby-Mori-Tanaka approach for vibrational behaviour of FG-CNTRC plate resting on elastic foundation [23]. They studied the effects of the CNT volume fraction, Winkler foundation modulus, shear elastic foundation modulus and various geometrical parameters on the vibration behavior of the FG-CNTR plates. Liew et al. conducted postbuckling behavior of carbon nanotube-

reinforced functionally graded cylindrical panels under axial compression using a meshless approach [24]. They eliminated shear locking using stabilized conforming nodal integration scheme and direct nodal integration method. Moreover, they used the modified Newton-Raphson method to trace the postbuckling path. The first known free vibration analysis of FG-CNTRC triangular plates using the FSDT was investigated based on a new meshfree method [25]. They presented new sets of vibration frequency parameters and mode shapes for various FG-CNTRC triangular plates.

Free vibration analysis of laminated FG-CNTRC rectangular plates was carried out using the *kp*-Ritz method based on FSDT[26] by Lei et al. They examined the effects of number of layers and lamination angle in detail. The stress distribution of FG-CNTRC cylinders was investigated by Moradi-Dastjerdi et al. they reported the effect of waviness and aspect ratio index of CNTs on the stress and displacement distribution of nanocomposites cylinders using a meshfree method. They concluded that waviness has a significant effect on the effective reinforcement of nanocomposites [27]. The effect of CNT waviness and aspect ratio on the buckling behaviour of functionally graded nanocomposite plate was established by Shams and Soltani [28]. They also investigated the effects of elastic foundations on the buckling behaviour of FG-CNTRC laminated plates using a meshfree method [29].

Free vibration of viscoelastic double-bonded polymeric nanocomposite plates reinforced by FG-CNTs were carried out by Mohammadimehr et al. using Hamilton's principle and sinusoidal shear deformation theory [30]. They determined natural frequency of nanocomposite plates by Navier's and meshless methods.

In this article, the effects of waviness and aspect ratio of CNTs on the buckling behaviour of cross-ply laminated composite plates composed of perfectly bonded CNTRC layers subjected to in-plane loads are analysed using the EFG based on FSDT. The Material properties of FG-CNTRCs are assumed to vary continuously along the plate thickness direction in each layer and estimated based on extended rule of mixture considering efficiency parameters accounting for size-dependence. Uniform and three types of functionally graded distributions of CNTs are considered. The principle of minimum potential energy is employed to obtain Galerkin weak-form formulation of the CNTRC plate. The full transformation method is applied to impose essential boundary conditions. The influences of volume fraction, waviness, types of distribution and aspect ratio of CNTs, width-to-thickness and aspect ratios of the plate on the buckling behaviour of CNTRC plates are investigated for different boundary conditions.

2 FUNCTIONALLY GRADED CARBON NANOTUBE-REINFORCED COMPOSITES

Consider a laminated CNTRC plate with length *a*, width *b* and thickness *h* (Fig. 1). The plate is made of a mixture from wavy SWCNTs and an isotropic matrix. The CNTs are either uniformly distributed (UD) or functionally graded (FG) along the thickness direction of each layer according to Eqs. (9) for UD, FG-V, FG-O and FG-X distribution types as shown in Fig. 2. Employing the extended rule of mixture the effective elastic properties of the CNTRC plate can be expressed as follows [10]

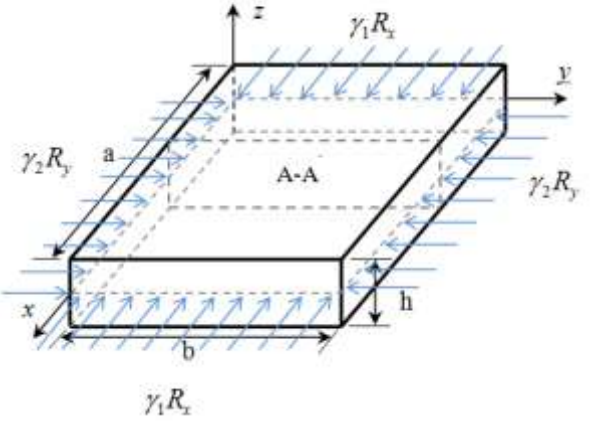

Fig. 1 Schematic configuration of a FG-CNTRC plate subjected to in-plane loads

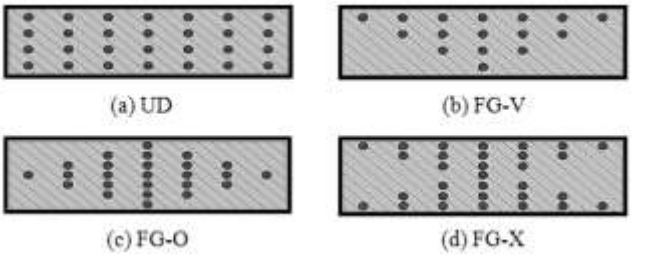

Fig. 2 Four type of CNT distributions: (a) UD, (b) FG-V, (c) FG-O and (d) FG-X in a nanocomposite layer

$$E_{11} = \eta_1 V_{CNT} E^{CNT}_{11,\eta^*} + V_m E^m, \tag{1}$$

$$\frac{\eta_2}{E_{22}} = \frac{V_{CNT}}{E^{CNT}_{22,\eta^*}} + \frac{V_m}{E^m}, \tag{2}$$

$$\frac{\eta_3}{G_{12}} = \frac{V_{CNT}}{G^{CNT}_{12,\eta^*}} + \frac{V_m}{G^m}, \tag{3}$$

$$\nu_{12} = V^*_{CNT} \nu^{CNT}_{12} + V_m \nu^m, \tag{4}$$

where E_{11,η^*}^{CNT}, E_{22,η^*}^{CNT}, G_{12,η^*}^{CNT} and ν_{12}^{CNT} denote effective Young's moduli, effective shear modulus and Poisson's ratio of the CNT, respectively. E^m, G^m and ν^m are the corresponding properties of the isotropic matrix. $\eta_j\,(j=1,2,3)$ are the CNT efficiency parameters accounting for the scale-dependent material properties evaluated by comparing the effective material properties obtained from MD simulations and that of numerical results obtained from the rule of mixture in [10]. V_{CNT} and V_m are the CNT and matrix volume fractions related by Eq. (5).

$$V_{CNT}+V_m=1. \tag{5}$$

The effective Young's moduli and shear modulus of wavy CNT are introduced as follows [31].

$$\begin{aligned} E_{ii,\eta^*}^{CNT} &= \eta^* E_{ii}^{CNT}, i=1,2 \\ G_{12,\eta^*}^{CNT} &= \eta^* G_{12}^{CNT} \end{aligned} \tag{6}$$

where

$$\begin{aligned} \eta^* &= 1-\frac{\tanh(K.AR/(1+<c>))}{K.AR/(1+<c>)} \\ K &= \sqrt{\frac{-2}{1+\nu_m}/\left(\frac{E_{11}^{CNT}}{E_{11}^{m}}\ln V_{CNT}\right)} \end{aligned} \tag{7}$$

The efficiency parameter, η^*, is considered to account the CNT aspect ratio and waviness [31]. *AR* is the aspect ratio of CNTs. $<c>$ is the average number of contacts for CNTs which depends on their aspect ratio defined as:

$$<c>= wV_{CNT}\left(4+\frac{3AR^2}{3AR+2}\right) \tag{8}$$

where the waviness, w, has been introduced for accounting the CNT's curvature within the CNTRC [31]. Introducing this parameter, the excluded volume due to the curvature of CNTs has been considered. The accuracy of this method has been investigated by [15] and [21]. The variation of CNT distribution through the plate is assumed as follows:

$$V_{CNT}=\begin{cases} V_{CNT}^* & (\text{UD CNTRC}), \\ \left(1+\dfrac{2z}{h}\right)V_{CNT}^* & (\text{FG-V CNTRC}), \\ 2\left(1-\dfrac{2|z|}{h}\right)V_{CNT}^* & (\text{FG-O CNTRC}), \\ 2\left(\dfrac{2|z|}{h}\right)V_{CNT}^* & (\text{FG-X CNTRC}), \end{cases} \tag{9}$$

where

$$V_{CNT}^{*}=\frac{w_{CNT}}{w_{CNT}+(\rho^{CNT}/\rho^{m})(1-w_{CNT})}. \tag{10}$$

V_{CNT}^* is the CNT volume fraction in which w_{CNT}, ρ^{CNT} and ρ^m are the mass fraction of CNTs, densities of CNTs and matrix, respectively. It should be noted that for both UD and FG cases, the values of mass fractions of CNTs are considered to be the same.

3 THE EFG FORMULATION

According to MLS approximation, an unknown function, $u(\mathbf{x})$, defined in the domain Ω can be approximated by $u^h(\mathbf{x})$ as [32].

$$u^h(\mathbf{x})=\sum_{j=1}^{m}p_j(\mathbf{x})a_j(\mathbf{x})=\mathbf{p}^{\mathrm{T}}(\mathbf{x})\mathbf{a}(\mathbf{x}), \tag{11}$$

in which $\mathbf{p}(\mathbf{x})$ is the basis function of spatial coordinates, $\mathbf{a}(\mathbf{x})$ is a vector of coefficients, and m is the number of basic functions. The quadratic bases commonly used are:

$$\begin{aligned} &\mathbf{p}^{\mathbf{T}}=[1,\mathrm{x},\mathrm{x}^2] && \text{in 1D, m = 3,} \\ &\mathbf{p}^{\mathbf{T}}=[1,\mathrm{x},\mathrm{y},\mathrm{x}^2,\mathrm{xy},\mathrm{y}^2] && \text{in 2D, m = 6.} \end{aligned} \tag{12}$$

The unknown coefficients $a_j(\mathbf{x})$ can be determined by minimizing the following weighted discrete L_2 norm.

$$J=\sum_{i=1}^{n}\bar{W}(\mathbf{x}-\mathbf{x}_i)[\mathbf{p}(\mathbf{x}_i)^{\mathrm{T}}\mathbf{a}(\mathbf{x})-\mathrm{u}_i]^2 \tag{13}$$

where $\bar{W}(\mathbf{x}-\mathbf{x}_i)$ or $\bar{W}_i(\mathbf{x})$ is the weight function associated with node i, n is the number of nodes in Ω, and u_i is the nodal parameter. Minimizing J in Eq. (13) with respect to $\mathbf{a}(\mathbf{x})$ leads to a set of linear equations as

$$\mathbf{A}(\mathbf{x})\mathbf{a}(\mathbf{x})=\mathbf{B}(\mathbf{x})\mathbf{u}, \tag{14}$$

where

$$\mathbf{A}(\mathbf{x})=\sum_{i=1}^{n}\bar{W}_i(\mathbf{x})\mathbf{p}(\mathbf{x}_i)\mathbf{p}^{\mathrm{T}}(\mathbf{x}_i) \tag{15}$$

$$\mathbf{B}(\mathbf{x})=[\bar{W}_1(\mathbf{x})\mathbf{p}(\mathbf{x}_1),\cdots,\bar{W}_n(\mathbf{x})\mathbf{p}(\mathbf{x}_n)]. \tag{16}$$

The coefficients $\mathbf{a}(\mathbf{x})$ are then obtained from Eq. (14)

$$\mathbf{a}(\mathbf{x})=\mathbf{A}^{-1}(\mathbf{x})\mathbf{B}(\mathbf{x})\mathbf{u}. \tag{17}$$

Substituting Eq. (15) into Eq. (11), the approximation $u^h(\mathbf{x})$ can be expressed in a standard form as:

$$u^h(\mathbf{x})=\sum_{i=1}^{n}\phi_i(\mathbf{x})u_i, \tag{18}$$

where the shape function for node *i*, denoted by $\phi_i(\mathbf{x})$ is given by Eq. (19).

$$\phi_i(\mathbf{x})=\sum_{j=1}^{m}p_j(\mathbf{x})\left(\mathbf{A}^{-1}(\mathbf{x})\mathbf{B}(\mathbf{x})\right)_{ji}=\mathbf{p}^{\mathrm{T}}\left(\mathbf{A}^{-1}\mathbf{B}\right)_i. \tag{19}$$

A quintic spline weight function is defined as:

$$\bar{W}_i(\mathbf{x}) = \begin{cases} 1-10\bar{r}_i^2+20\bar{r}_i^3-15\bar{r}_i^4+4\bar{r}_i^5; & 0\le \bar{r}_i <1 \\ 0 & ; \quad \bar{r}_i \ge 1 \end{cases}, \tag{20}$$

where

$$\bar{r}_i = \frac{|\mathbf{x}-\mathbf{x}_i|}{d_s}, \tag{21}$$

in which $|\mathbf{x}-\mathbf{x}_i|$ is the distance from node $\mathbf{x}_i$ to the sampling point $\mathbf{x}$, and d_s is the size of support domain for the sampling point $\mathbf{x}$.

4 LAMINATED COMPOSITE PLATES REINFORCED BY CARBON NANOTUBES

Employing the FSDT for a laminated plate composed of CNTRC layers, the displacement field of the plate can be expressed as [11].

$$u(x,y,z) = u_0(x,y) + z\varphi_x(x,y), \tag{22}$$

$$v(x,y,z) = v_0(x,y) + z\varphi_y(x,y), \tag{23}$$

$$w(x,y,z) = w_0(x,y), \tag{24}$$

where (u,v,w) are the displacements of an arbitrary point (x,y,z) in the domain laminated composite plate along x-, y- and z- directions, respectively. (u_0,v_0,w_0) represent the displacements of a point at the mid-plane of the plate and (φ_x,φ_y) denote rotations of the unit normal to the mid-plane of the plate at the martial point (x,y) about positive y- and negative x- axes, respectively. The strain-displacement equations of the plate are given by:

$$\boldsymbol{\varepsilon} = \boldsymbol{\varepsilon}^{(0)} + z\boldsymbol{\varepsilon}^{(1)}, \tag{25}$$

$$\boldsymbol{\gamma} = \boldsymbol{\gamma}^{(0)}, \tag{26}$$

where

$$\boldsymbol{\varepsilon} = [\varepsilon_{xx} \quad \varepsilon_{yy} \quad \gamma_{xy}]^{\mathrm{T}}, \boldsymbol{\gamma} = [2\varepsilon_{yz} \quad 2\varepsilon_{xz}]^{\mathrm{T}}, \tag{27}$$

and

$$\boldsymbol{\varepsilon}^{(0)} = \begin{Bmatrix} \dfrac{\partial u_0}{\partial x} \\ \dfrac{\partial v_0}{\partial y} \\ \dfrac{\partial u_0}{\partial y}+\dfrac{\partial v_0}{\partial x} \end{Bmatrix}, \boldsymbol{\varepsilon}^{(1)} = \begin{Bmatrix} \dfrac{\partial \varphi_x}{\partial x} \\ \dfrac{\partial \varphi_y}{\partial y} \\ \dfrac{\partial \varphi_x}{\partial y}+\dfrac{\partial \varphi_y}{\partial x} \end{Bmatrix}, \tag{28}$$

and

$$\boldsymbol{\gamma}^{(0)} = \begin{Bmatrix} \varphi_y + \dfrac{\partial w_0}{\partial y} \\ \varphi_x + \dfrac{\partial w_0}{\partial x} \end{Bmatrix}. \tag{29}$$

Then, the constitutive relations are expressed as [33].

$$\begin{Bmatrix} \sigma_{xx} \\ \sigma_{yy} \\ \sigma_{xy} \\ \sigma_{xz} \\ \sigma_{yz} \end{Bmatrix} = \begin{bmatrix} \bar{Q}_{11}(z) & \bar{Q}_{12}(z) & \bar{Q}_{16}(z) & 0 & 0 \\ \bar{Q}_{12}(z) & \bar{Q}_{22}(z) & \bar{Q}_{26}(z) & 0 & 0 \\ \bar{Q}_{16}(z) & \bar{Q}_{26}(z) & \bar{Q}_{66}(z) & 0 & 0 \\ 0 & 0 & 0 & \bar{Q}_{55}(z) & \bar{Q}_{45}(z) \\ 0 & 0 & 0 & \bar{Q}_{45}(z) & \bar{Q}_{44}(z) \end{bmatrix} \begin{Bmatrix} \varepsilon_{xx} \\ \varepsilon_{yy} \\ 2\varepsilon_{xy} \\ 2\varepsilon_{xz} \\ 2\varepsilon_{yz} \end{Bmatrix}, \tag{30}$$

where

$$\left[\bar{Q}\right] = [\mathrm{T}][Q][\mathrm{T}]^T, \tag{31}$$

in which

$$[Q] = \begin{bmatrix} Q_{11}(z) & Q_{12}(z) & 0 & 0 & 0 \\ Q_{12}(z) & Q_{22}(z) & 0 & 0 & 0 \\ 0 & 0 & Q_{66}(z) & 0 & 0 \\ 0 & 0 & 0 & Q_{55}(z) & 0 \\ 0 & 0 & 0 & 0 & Q_{44}(z) \end{bmatrix}, \tag{32}$$

$$[\mathrm{T}] = \begin{bmatrix} m^2 & n^2 & -2mn & 0 & 0 \\ n^2 & m^2 & 2mn & 0 & 0 \\ mn & -mn & (\mathrm{m}^2-n^2) & 0 & 0 \\ 0 & 0 & 0 & m & n \\ 0 & 0 & 0 & -n & m \end{bmatrix} \tag{33}$$

And

$$Q_{11} = \frac{E_{11}}{1-\nu_{12}\nu_{21}}, Q_{22} = \frac{E_{22}}{1-\nu_{12}\nu_{21}}, Q_{12} = \frac{\nu_{21}E_{11}}{1-\nu_{12}\nu_{21}}, \tag{34}$$
$$Q_{44} = G_{23}, Q_{55} = G_{13}, Q_{66} = G_{12}.$$

Here $m=\cos\theta$, $n=\sin\theta$ and θ is the angle between the material and the plate coordinate systems. E_{11} and E_{22} are the effective Young's moduli of CNTRC plate in the principle material coordinates; G_{12}, G_{13} and G_{23} are the shear moduli, and ν_{12} and ν_{21} are the Poisson's ratios. Note that $\nu_{21}=(E_{22}/E_{11})\nu_{12}$. According to FSDT, the relation between the stress resultants and the strains can be written as:

$$\begin{Bmatrix} \mathbf{N} \\ \mathbf{M} \\ \mathbf{Q}^{\mathbf{s}} \end{Bmatrix} = \begin{bmatrix} \mathbf{A} & \bar{\mathbf{B}} & \mathbf{0} \\ \bar{\mathbf{B}} & \mathbf{D} & \mathbf{0} \\ \mathbf{0} & \mathbf{0} & \mathbf{A}^{\mathbf{s}} \end{bmatrix} \begin{Bmatrix} \boldsymbol{\varepsilon}^{(0)} \\ \boldsymbol{\varepsilon}^{(1)} \\ \boldsymbol{\gamma}^{(0)} \end{Bmatrix}, \tag{35}$$

where the in-plane force, moment and transverse force resultants are defined as:

$$(\mathbf{N},\mathbf{M}) = \begin{pmatrix} N_{xx}, M_{xx} \\ N_{yy}, M_{yy} \\ N_{xy}, M_{xy} \end{pmatrix} = \int_{-h/2}^{h/2} (1, \mathrm{z}) \begin{pmatrix} \sigma_{xx} \\ \sigma_{yy} \\ \sigma_{xy} \end{pmatrix} dz, \tag{36}$$

$$\mathbf{Q}^{\mathbf{s}} = \begin{Bmatrix} Q_y^s \\ Q_x^s \end{Bmatrix} = \int_{-h/2}^{h/2} \begin{Bmatrix} \sigma_{yz} \\ \sigma_{xz} \end{Bmatrix} dz, \tag{37}$$

The components of extensional $\mathbf{A}$, bending-extensional coupling $\bar{\mathbf{B}}$, bending $\mathbf{D}$ and transverse shear stiffness $\mathbf{A}^{\mathbf{s}}$ are defined as:

$$\left(A_{ij}, \bar{B}_{ij}, D_{ij}\right) = \int_{-h/2}^{h/2} \bar{Q}_{ij} \left(1, z, z^2\right) dz \quad \text{for } i, j = 1, 2 \text{ and } 6, \tag{38}$$

$$A_{ij}^s = \kappa \int_{-h/2}^{h/2} \bar{Q}_{ij} dz \quad \text{for } i, j = 4 \text{ and } 5. \tag{39}$$

κ are the modified shear correction factors which is suggested to be obtained from the following relation [34].

$$\kappa = \frac{5}{6 - \nu_{12}}. \tag{40}$$

Total potential energy of the CNTRC plate is expressed as [11].

$$\mathbf{\Pi} = \mathbf{U}_p - \mathbf{W}, \tag{41}$$

where $\mathbf{U}_p$ and $\mathbf{W}$ denote the strain energy of the plate and the work done by external forces, respectively. The strain energy of the plate can be written as

$$\mathbf{U}_p = \frac{1}{2} \int_\Omega \boldsymbol{\varepsilon}_p^{\mathrm{T}} \mathbf{S}_p \, \boldsymbol{\varepsilon}_p \, d\Omega, \tag{42}$$

where

$$\boldsymbol{\varepsilon}_p = \begin{Bmatrix} \boldsymbol{\varepsilon}^{(0)} \\ \boldsymbol{\varepsilon}^{(1)} \\ \boldsymbol{\gamma}^{(0)} \end{Bmatrix}, \mathbf{S}_p = \begin{bmatrix} \mathbf{A} & \bar{\mathbf{B}} & \mathbf{0} \\ \bar{\mathbf{B}} & \mathbf{D} & \mathbf{0} \\ \mathbf{0} & \mathbf{0} & \mathbf{A}^{\mathbf{s}} \end{bmatrix}. \tag{43}$$

Considering the in-plane loads, $\gamma_1 R_x$ and $\gamma_2 R_y$ as depicted in Fig. 1 applied on the plate, $\mathbf{W}$ can be expressed as:

$$\mathbf{W} = \int_\Omega \begin{bmatrix} \dfrac{\partial w}{\partial x} & \dfrac{\partial w}{\partial y} \end{bmatrix} \begin{bmatrix} \gamma_1 R_x & 0 \\ 0 & \gamma_2 R_y \end{bmatrix} \begin{bmatrix} \dfrac{\partial w}{\partial x} \\ \dfrac{\partial w}{\partial y} \end{bmatrix} d\Omega. \tag{44}$$

Substituting Eqs. (42) and (44) into Eq. (41) and following the standard procedure of EFG, the following system of eigenvalue equations is derived.

$$(\mathbf{K} - \lambda \mathbf{K}^g)\mathbf{u} = \mathbf{0}, \tag{45}$$

where λ is the critical buckling load of the plate, $\mathbf{K}^g$ is the geometric stiffness matrix and $\mathbf{K}$ denotes the global stiffness matrices of the plate given by:

$$\mathbf{K}^p = \mathbf{K}^m + \mathbf{K}^b + \mathbf{K}^s + \mathbf{K}^c, \tag{46}$$

$$\mathbf{K}_{ij}^m = \int_\Omega \mathbf{B}_i^{m^T} \mathbf{A} \mathbf{B}_j^m d\Omega, \tag{47}$$

$$\mathbf{K}_{ij}^b = \int_\Omega \mathbf{B}_i^{b^T} \mathbf{D} \mathbf{B}_j^b d\Omega, \tag{48}$$

$$\mathbf{K}_{ij}^s = \int_\Omega \mathbf{B}_i^{s^T} \mathbf{A}^{\mathbf{s}} \mathbf{B}_j^s d\Omega, \tag{49}$$

$$\mathbf{K}_{ij}^c = \int_\Omega \mathbf{B}_i^{m^T} \bar{\mathbf{B}} \mathbf{B}_j^b d\Omega + \int_\Omega \mathbf{B}_i^{b^T} \bar{\mathbf{B}} \mathbf{B}_j^m d\Omega, \tag{50}$$

$$\mathbf{K}_{ij}^g = \int_\Omega \mathbf{H}_i^{\mathbf{T}} \mathbf{R} \mathbf{H}_j d\Omega, \tag{51}$$

in which

$$\mathbf{B}^m = \begin{bmatrix} \phi_{i,x} & 0 & 0 & 0 & 0 \\ 0 & \phi_{i,y} & 0 & 0 & 0 \\ \phi_{i,y} & \phi_{i,x} & 0 & 0 & 0 \end{bmatrix}, \tag{52}$$

$$\mathbf{B}^b = \begin{bmatrix} 0 & 0 & 0 & \phi_{i,x} & 0 \\ 0 & 0 & 0 & 0 & \phi_{i,y} \\ 0 & 0 & 0 & \phi_{i,y} & \phi_{i,x} \end{bmatrix}, \tag{53}$$

$$\mathbf{B}^s = \begin{bmatrix} 0 & 0 & \phi_{i,y} & 0 & \phi_i \\ 0 & 0 & \phi_{i,x} & \phi_i & 0 \end{bmatrix}, \tag{54}$$

$$\mathbf{H} = \begin{bmatrix} 0 & 0 & \phi_{i,x} & 0 & 0 \\ 0 & 0 & \phi_{i,y} & 0 & 0 \end{bmatrix}, \tag{55}$$

$$\mathbf{R} = \begin{bmatrix} \gamma_1 R_x & 0 \\ 0 & \gamma_2 R_y \end{bmatrix}. \tag{56}$$

5 BOUNDARY CONDITIONS

The essential boundary conditions cannot be directly imposed in EFG method due to the fact that the shape functions do not satisfy the Kronecker delta property. Several approaches are used to impose boundary conditions including the Lagrangian multiplier method [35] and the penalty method [36]. The adopted method used in this paper is the full transformation method proposed by Chen et al. [37] and has been used by many researchers, e.g. [16],[17] and [38] due to its good accuracy and simple implementation. The boundary conditions considered in this study are as follows.

Simply supported (S):

$$\begin{aligned} &v_0 = w_0 = \varphi_y = 0, \text{ at } x = 0, a, \\ &u_0 = w_0 = \varphi_x = 0, \text{ at } y = 0, b. \end{aligned} \tag{57}$$

Clamped (C):

$$v_0 = w_0 = \varphi_x = \varphi_y = 0, \text{ at } x = 0, a,$$
$$u_0 = w_0 = \varphi_x = \varphi_y = 0, \text{ at } y = 0, b. \quad (58)$$

The supports of the plate edges are denoted by S and C for simply supported and clamped boundary conditions, respectively.

6 NUMERICAL RESULTS AND DISCUSSION

In this study for validation of presented method, the buckling load parameters of two types of isotropic and single layer CNTRC rectangular plates are carried out and compared with previous studies. In the second step, several parametric studies are presented and investigated in detail to reveal the influences of CNT volume fraction, waviness and aspect ratio, plate width-to-thickness, plate aspect ratio and boundary conditions on the buckling characteristics of the plates composed of FG-CNTRC layers.

The buckling problem of isotropic plates with various boundary conditions under compressive loads is presented to investigate the convergency and accuracy of the present method. The results are listed in Table 1 for a plate using various node schemes. The results are compared with that of presented by Lam et al. [39]. As can be seen, the solution converges when the number of nodes is increased and the results are converged with regular nodal distribution. Accordingly, this node scheme is used for discretization of the domain in the following studies.

Table 1 Convergence study of buckling load parameters $(\bar{N}_{cr} = N_{cr} / \pi^2)$ for an isotropic square plate subjected to uniaxial ($\kappa = 5/6, \nu = 0.3$).

	Number of Nodes	Uniaxial		Biaxial	
		SSSS	SCSC	SSSS	SCSC
Present	13×13	4.005	7.691	2.003	3.834
	15×15	4.003	7.695	2.004	3.827
	17×17	4.003	7.687	2.004	3.831
	19×19	3.999	7.693	2.002	3.832
	21×21	3.996	7.692	2.001	3.830
Ref [36]		4.000	7.691	2.000	3.830

The accuracy of presented method is also examined by performing a comparison study of buckling load parameters $(\bar{N}_{cr} = N_{cr} b^2 / E^m \mathrm{h}^3)$ of a CNTRC square plate with all edges simply supported (SSSS) subjected to the uniaxial compression $(\gamma_1 = -1, \gamma_2 = 0)$, biaxial compression $(\gamma_1 = -1, \gamma_2 = -1)$ and biaxial compression and tension $(\gamma_1 = -1, \gamma_2 = 1)$ with the obtained result in [17]. Buckling load parameters are presented in Table 2 for the first four modes. The geometrical and material properties of the plate are considered as mentioned in [17]. It can be seen that the obtained results are in good agreement with the results obtained in [17].

Table 2 Comparison study of buckling load parameters $(\bar{N}_{cr} = N_{cr} b^2 / E^m \mathrm{h}^3)$ for a simply supported CNTRC square plate subjected to uniaxial and biaxial in-plane loads ($V_{CNT} = 0.11, b/h = 20$).

Mode		$\gamma_1 = -1, \gamma_2 = 0$	$\gamma_1 = -1, \gamma_2 = -1$	$\gamma_1 = -1, \gamma_2 = 1$
1	Present	31.1569	9.5621	90.0966
	Ref [17]	30.9076	9.3805	89.9909
2	Present	47.9741	10.6660	101.2563
	Ref [17]	46.9779	10.3981	101.0670
3	Present	70.5573	14.5639	108.1136
	Ref [17]	69.3955	14.0470	107.7075
4	Present	76.3942	15.5778	109.3287
	Ref [17]	74.5610	15.3108	109.0635

After validation of the proposed method, the buckling analysis of a laminated FG-CNTRC rectangular plate subjected to various in-plane loads is investigated. In the following studies, Poly-co-vinylene, referred to as PmPV and armchair (10, 10) SWCNTs are selected as the matrix and the reinforcement materials, respectively.

The CNTs are distributed uniformly and functionally graded in the polymer matrix of each layer. The material properties of CNTs and PmPV are listed in Table 3. Values of $\eta_i (i = 1, 2 \text{ and } 3)$ for different CNT volume fractions are presented in Table 4. Note that $\eta_3 = \eta_2$, and $G_{13} = G_{12}$.

Table 3 Elastic properties of the (10, 10) SWCNT and the polymer matrix [10].

SWCNT	Polymer matrix
$E_{11} = 5.6466 (\mathrm{TPa})$	$E_m = 2.1 (\mathrm{GPa})$
$E_{22} = 7.0800 (\mathrm{TPa})$	
$G_{12} = 1.9447 (\mathrm{TPa})$	
$\nu_{12} = 0.175$	$\nu_m = 0.34$

Table 4 CNT efficiency parameters for different values of volume fractions [10].

V^*_{CNT}	η_1	η_2	η_3
0.11	0.149	0.934	0.934
0.14	0.150	0.941	0.941
0.17	0.149	1.381	1.381

$G_{23} = G_{12}$ following the assumptions mentioned in [10]. The plate thickness is taken to be $h = 2 (\mathrm{mm})$ in all case studies. Hereafter, it is assumed that for the laminated plate all layers have the same material properties and thickness.

Table 5 shows the buckling load parameters $(N_{cr}^{*} = N_{cr}b^2 / E_m h^3)$ for four types of CNT distribution of simply supported cross-ply $[0^\circ / 90^\circ / 0^\circ / 90^\circ / 0^\circ]$ laminated CNTRC square plates with the CNT aspect ratio, $AR = 50$, plate width-to-thickness ratio, $b/h = 10$, different values of CNT waviness parameter $w(= 0, 0.5, 1 \text{and} 2)$ and volume fraction $V_{CNT}^{*}(= 0.11, 0.14 \text{and} 0.17)$. The CNTRC plates are subjected to uniaxial compressive load $(\gamma_1 = -1, \gamma_2 = 0)$. The numerical results show that CNTs volume fraction has significant influence on the buckling load parameters of the CNTRC plates. Moreover, it can be observed that the laminated FG-X CNTRC plates have the highest value of buckling load parameter while the laminated UD CNTRC plates have the lowest one in all CNT volume fractions and waviness parameters. This behaviour can be justified by the fact that in an FG-X CNT arrangement, the CNTs are denser close to the top and bottom of the CNTRC plate which leads to higher plate stiffness. Moreover, Table 5 reveals that increasing in the waviness parameter leads to decrease in buckling load parameters of CNTRC plates. Furthermore, the influence of CNTs waviness on buckling load parameters of the plate is alleviated as increase irrespective of their CNT volume fractions and distributions. It can be seen that the maximum values of buckling load parameters belongs to straight CNT i.e. $w = 0$.

Table 5 Buckling load parameters $(N_{cr}^{*} = N_{cr}b^2 / E_m h^3)$ of simply supported cross-ply $[0^\circ / 90^\circ / 0^\circ / 90^\circ / 0^\circ]$ laminated CNTRC square plate for various CNT volume fractions and $(b/h = 10, AR = 50)$.

V_{CNT}	w	UD	FG-V	FG-O	FG-X
0.11	0	8.3121	8.7632	8.6931	8.9444
	0.5	3.8753	3.8510	3.8449	3.8579
	1	3.6169	3.6213	3.6173	3.6253
	2	3.4964	3.4782	3.4768	3.4833
0.14	0	10.1723	10.8447	10.7579	11.1029
	0.5	3.9588	3.9541	3.9471	3.9637
	1	3.6892	3.7019	3.6960	3.7072
	2	3.5379	3.5053	3.5058	3.5111
0.17	0	13.8978	14.9669	14.8469	15.3366
	0.5	5.5071	5.5523	5.5353	5.5674
	1	5.2753	5.3089	5.2939	5.3233
	2	5.0367	4.9581	4.9558	4.9649

In the next model, the previous model is considered with the CNT waviness parameter, $w = 0$, for various values of CNT aspect ratio, AR, and volume fractions, V_{CNT}^{*}. Comparing the results in Table 6 reported for SSSS boundary conditions reveals that the buckling load parameters $(N_{cr}^{*} = N_{cr}b^2 / E_m h^3)$ of the CNTRC plates inclined by increasing CNT aspect ratio and tend to reach constant values as AR increases.

Table 6 Buckling load parameters $(N_{cr}^{*} = N_{cr}b^2 / E_m h^3)$ of simply supported cross-ply $[0^\circ / 90^\circ / 0^\circ / 90^\circ / 0^\circ]$ laminated CNTRC square plate for different values of CNT volume fraction and aspect ratio under uniaxial compressive load $(b/h = 10, w = 0)$.

V_{CNT}	AR	UD	FG-V	FG-O	FG-X
0.11	50	8.3121	8.7632	8.6931	8.9444
	100	14.1724	14.5866	14.4879	14.9349
	500	21.7849	21.7470	21.6291	22.2199
	1000	22.6427	22.5568	22.4370	23.0377
0.14	50	10.1723	10.8447	10.7579	11.1029
	100	17.2673	17.8232	17.7111	18.2685
	500	25.4987	25.5032	25.3719	26.0519
	1000	26.3948	26.3459	26.2120	26.9022
0.17	50	13.8978	14.9669	14.8469	15.3366
	100	23.2869	24.1674	24.0060	24.7837
	500	34.1122	34.1950	34.0111	34.9589
	1000	35.3175	35.3229	35.1350	36.0966

The effects of boundary conditions on the buckling behaviour of cross-ply $[0^\circ / 90^\circ / 0^\circ]$ laminated UD and FG-CNTRC square plates under uniaxial $(\gamma_1 = -1, \gamma_2 = 0)$ compressive loads are investigated in Table 7 for three types of boundary conditions. The CNT volume fraction, CNT aspect ratio, waviness parameter and plate with-to-thickness ratio are considered to be $V_{CNT}^{*} = 0.11$, $AR = 50$, $w = 0$ and, $b/h = 10$, respectively. It can be seen that as more constrains are applied on the edges of the plate the, buckling load parameters are increased. Thus the lowest and the highest values of buckling load parameters occurred in SSSS and CCCC boundary conditions, respectively.

Table 7 First four buckling load parameters $(\bar{N}_{cr} = N_{cr}b^2 / E^m h^3)$ of cross-ply $[0^\circ / 90^\circ / 0^\circ]$ laminated CNTRC square plate under uniaxial compression $(V_{CNT}^{*} = 0.11, b/h = 10, AR = 50, w = 0)$.

	Mode	SSSS	SCSC	CCCC
UD	1	8.1231	11.9691	19.3691
	2	16.3129	17.2609	21.8661
	3	22.4790	23.1161	27.5189
	4	22.7166	26.2297	28.4841
FG-V	1	8.4469	12.2011	19.9019
	2	16.9180	17.8449	22.4101
	3	23.0127	23.7096	28.0144
	4	23.3171	26.7018	28.9199
FG-O	1	8.2549	11.7911	19.5637
	2	16.7345	17.6123	22.2121
	3	22.5771	23.5398	27.8473
	4	23.1640	26.1219	28.7200
FG-X	1	8.9411	13.3013	20.8941
	2	17.4909	18.5519	23.0272
	3	23.8221	24.2654	28.5277
	4	24.0639	11.9687	19.3699

It can also be observed that buckling load parameter of all edges simply supported CNTRC plates depends on CNT distribution type more than other two types of boundary conditions.

The dependency of buckling load parameters $(\bar{N}_{cr} = N_{cr}b^2 / E^m h^3)$ to the aspect ratio (a/b) of the cross-ply $[0^\circ/90^\circ/0^\circ/90^\circ/0^\circ]$ laminated CNTRC square plates subjected to biaxial compression $(\gamma_1 = -1, \gamma_2 = -1)$ is delineated in Figs. 3 for SSSS boundary conditions. Two cases of UD and FG-X CNT distribution are considered with CNT aspect ratio, $AR = 50$, plate width-to-thickness, $b/h = 10$, waviness parameter, $w = 1$ and different CNT volume fraction, $V^*_{CNT} = 0.11, 0.14 \text{ and } 0.17$. This figure discloses that increase in the value of a/b leads to decrease in the values of buckling load parameter of CNTRC.

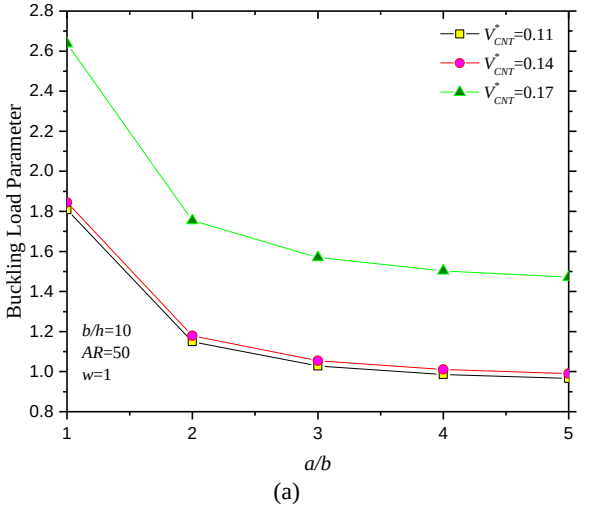

(a)

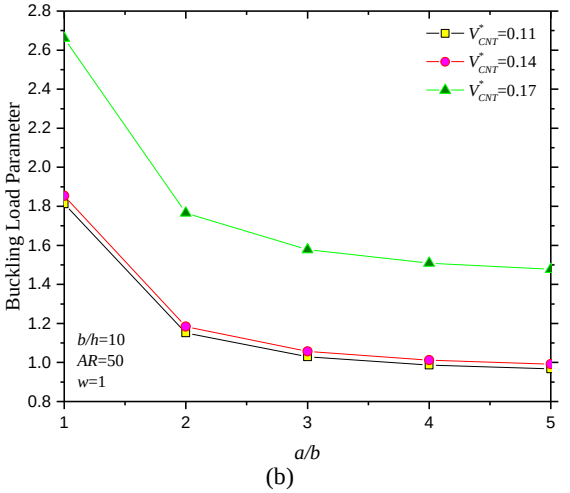

(b)

Fig. 3 Variation of the buckling load parameters $(N^*_{cr} = N_{cr}b^2 / E_m h^3)$ versus aspect ratios of simply supported cross-ply $[0^\circ/90^\circ/0^\circ/90^\circ/0^\circ]$ laminated a) UD b) FG-X CNTRC square plates subjected to biaxial compression $(\gamma_1 = -1, \gamma_2 = -1)$.

The variation of buckling load parameters $(\bar{N}_{cr} = N_{cr}b^2 / E^m h^3)$ of simply supported cross-ply $[0^\circ/90^\circ/0^\circ/90^\circ/0^\circ]$ laminated CNTRC square plates under biaxial $(\gamma_1 = -1, \gamma_2 = -1)$ in-plane loads versus plate width-to-thickness ratio, b/h, are depicted in Figs. 4 with three cases of CNT volume fractions, i.e. $V^*_{CNT} = 0.11, 0.14, \text{and } 0.17$, for UD and FG-X CNT distributions. As expected, by increasing the plate width-to-thickness ratio, b/h, the buckling load parameters are increased for all in-plane load conditions. In addition, the dependency of the plate buckling load parameters on width-to-thickness ratio of the plate declined when b/h increases.

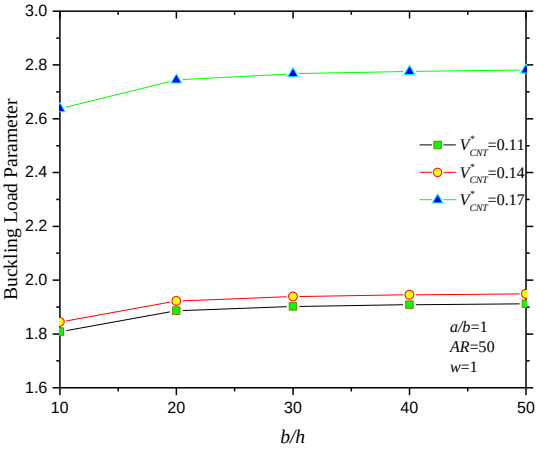

(a)

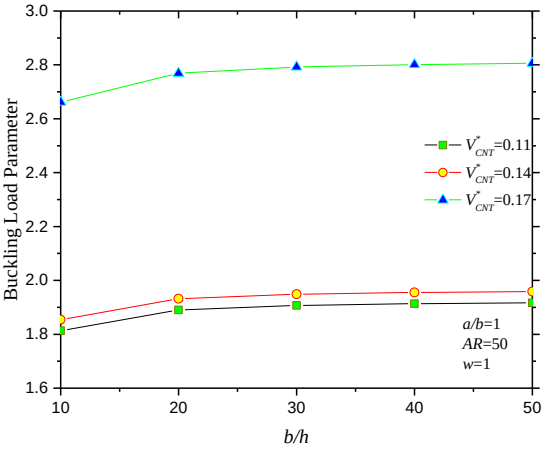

(b)

Fig. 4 Variation of the buckling load parameters $(N^*_{cr} = N_{cr}b^2 / E_m h^3)$ versus width-to-thickness aspect ratios of simply supported cross-ply $[0^\circ/90^\circ/0^\circ/90^\circ/0^\circ]$ laminated a) UD b) FG-X CNTRC square plates subjected to biaxial compression $(\gamma_1 = -1, \gamma_2 = -1)$.

7 CONCLUSION

In the present study, buckling analysis of laminated FG-CNTRC plates is investigated based on FSDT us the EFG. The laminated plate is composed of perfectly bonded FG-CNTRC layers. The effective material properties of the plate are estimated based on a micromechanical model and the extended rule of mixture to consider the scale-dependent material properties. The effects of various types of CNT distribution types, waviness, aspect ratio and volume fraction, plate width-to thickness and aspect ratio and boundary conditions on the buckling behaviour of the laminated nanocomposite plates are studied.

REFERENCES

[1] Lau , K. T. and Hui, D., "The revolutionary creation of new advanced materials—carbon nanotube composites," Composite Part B Engineeeing., Vol. 33, No. 4, 2002, pp. 263–277.

[2] Thostenson, E. T., Ren, Z., and Chou, T.-W., "Advances in the science and technology of carbon nanotubes and their composites: a review," Composite Science and Technology, Vol. 61, No. 13, Oct. 2001, pp. 1899–1912.

[3] Esawi, A. K. K. and Farag, M. M., "Carbon nanotube reinforced composites: Potential and current challenges," Materials and Design, Vol. 28, No. 9, Jan. 2007, pp. 2394–2401.

[4] Odegard, G., "Constitutive modeling of nanotube–reinforced polymer composites," Composite Science Technology, Vol. 63, No. 11, Aug. 2003, pp. 1671–1687.

[5] Griebel, M. and Hamaekers, J., "Molecular dynamics simulations of the elastic moduli of polymer–carbon nanotube composites," Comput. Methods Applied Mech. Engineering, Vol. 193, No. 17–20, May 2004 , pp. 1773–1788.

[6] Qian, D., Dickey, E. C., Andrews, R., Rantell, T., and Company, C., "Load transfer and deformation mechanisms in carbon nanotube-polystyrene composites," Applied Physics Letters, Vol. 76, No. 20, 2000, pp. 2868–2870.

[7] Ruan, S. L., Gao, P., Yang, X. G., and Yu, T. X., "Toughening high performance ultrahigh molecular weight polyethylene using multiwalled carbon nanotubes," Polymer (Guildf)., Vol. 44, No. 19, 2003 , pp. 5643–5654.

[8] Jafari Mehrabadi, S., Sobhani Aragh, B., Khoshkhahesh, V., and Taherpour, A., "Mechanical buckling of nanocomposite rectangular plate reinforced by aligned and straight single-walled carbon nanotubes," Composiote Part B: Engineering, Vol. 43, No. 4, Jun. 2012, pp. 2031–2040.

[9] Malekzadeh, P. and Shojaee, M., "Buckling analysis of quadrilateral laminated plates with carbon nanotubes reinforced composite layers," Thin-Walled Structures, Vol. 71, Oct. 2013, pp. 108–118.

[10]Shen, H.S., "Nonlinear bending of functionally graded carbon nanotube-reinforced composite plates in thermal environments," Composite Structures, Vol. 91, No. 1, Nov. 2009, pp. 9–19.

[11]Zhu, P., Lei, Z. X., and Liew, K. M., "Static and free vibration analyses of carbon nanotube-reinforced composite plates using finite element method with first order shear deformation plate theory," Composite Structures, Vol. 94, No. 4, Mar. 2012, pp. 1450–1460.

[12]Sobhani Aragh, B., Nasrollah Barati, A. H., and Hedayati, H., "Eshelby–Mori–Tanaka approach for vibrational behavior of continuously graded carbon nanotube-reinforced cylindrical panels," Compos. Part B: Engineering, Vol. 43, No. 4, Jun. 2012, pp. 1943–1954.

[13]Alibeigloo, A. and Liew, K. M., "Thermoelastic analysis of functionally graded carbon nanotube-reinforced composite plate using theory of elasticity," Composite Structures, Vol. 106, Dec. 2013, pp. 873–881.

[14]Moradi-Dastjerdi, R., Foroutan, M., Pourasghar, A., and Sotoudeh-Bahreini, R., "Static analysis of functionally graded carbon nanotube-reinforced composite cylinders by a mesh-free method," Journal of Reinforced Plastic Composites., Vol. 32, No. 9, Feb. 2013, pp. 593–601.

[15]Moradi-Dastjerdi, R., Foroutan, M., and Pourasghar, A., "Dynamic analysis of functionally graded nanocomposite cylinders reinforced by carbon nanotube by a mesh-free method," Materials and Design, Vol. 44, Feb. 2013, pp. 256–266.

[16]Lei , Z. X., Liew , K. M., and Yu , J. L., "Large deflection analysis of functionally graded carbon nanotube-reinforced composite plates by the element-free kp-Ritz method," Computer Methods in Applied Mechanics and Engineering, Vol. 256, Apr. 2013, pp. 189–199.

[17]Lei , Z. X., Liew, K. M., and Yu , J. L., "Buckling analysis of functionally graded carbon nanotube-reinforced composite plates using the element-free kp-Ritz method," Composite Structures, Vol. 98, Apr. 2013, pp. 160–168.

[18]Shen , H. S., and Xiang. Y., "Nonlinear vibration of nanotube-reinforced composite cylindrical panels resting on elastic foundations in thermal environments," Composite Structures, Vol. 111, 2014, pp. 291–300.

[19]Shen , H. S, "Thermal buckling and postbuckling of functionally graded fiber reinforced composite laminated plates," Journal of Composite Materials, Vol. 47, No. August 2012, 2012, pp. 2783–2795.

[20]Jam, J. E., Kia, S. M., Ghorbanpour Arani, A., and Emdadi, M., "Elastic buckling of circular annular plate reinforced with carbon nanotubes," Polymer Composites, Vol. 32, No. 6, Jun. 2011 , pp. 896–903.

[21]Jam , J. E., Pourasghar , A., and Kamarian , S., "Effect of the aspect ratio and waviness of carbon nanotubes on the vibrational behavior of functionally graded nanocomposite cylindrical panels," Polymer Composites, Vol. 33, No. 11, Nov. 2012 , pp. 2036–2044.

[22]Asadi E. and Jam, J., "Analytical and Numerical Buckling Analysis of Carbon Nanotube Reinforced Annular Composite Plates," International Journal of Advanced Design and Manufacturing Technology, Vol. 7, No. 2, 2014, pp. 35–44.

[23]Kamarian , S., Pourasghar, A., and Yas, M., "Eshelby-Mori-Tanaka approach for vibrational behavior of functionally graded carbon nanotube-reinforced plate resting on elastic foundation," Journal of Mechanical Science and Technology, Vol. 27, No. 11, Nov. 2013 , pp. 3395–3401.

[24]Liew, K. M., Lei, Z. X., Yu, J. L., and Zhang, L. W., "Postbuckling of carbon nanotube-reinforced functionally graded cylindrical panels under axial compression using a meshless approach," Computer Methods in Applied Mechanics and Engineering, Vol. 268, Jan. 2014, pp. 1–17.

[25]Zhang, L. W., Lei, Z. X., and Liew, K. M., "Free vibration analysis of functionally graded carbon nanotube-reinforced composite triangular plates using the FSDT and element-free IMLS-Ritz method," Composite Structures, Vol. 120, 2015, pp. 189–199.

[26]Lei, Z. X., Zhang, L. W., and Liew, K. M., "Free vibration analysis of laminated FG-CNT reinforced composite rectangular plates using the kp-Ritz method," Composite Structures, Vol. 127, 2015, pp. 245–259.

[27]Moradi-Dastjerdi, R., Sheikhi, M. M., and Shamsolhoseinian, H. R., "Stress Distribution in Functionally Graded Nanocomposite Cylinders Reinforced by Wavy Carbon Nanotube," International Journal of Advanced Design and Manufacturing Technology, Vol. 7, No. 4, 2014, pp. 43–54.

[28]Shams, Sh. and Soltani, B., "The Effects of Carbon Nanotube Waviness and Aspect Ratio on the Buckling Behavior of Functionally Graded Nanocomposite Plates Using a Meshfree Method," Polymer Composites, DOI 10.1002/pc.23814, Oct. 2015.

[29]Shams, Sh. and Soltani, B., "Buckling of Laminated Carbon Nanotube-Reinforced Composite Plates on Elastic Foundations Using a Meshfree Method," Arabian Journal of Science and Engineering, Vol. 41, No. 5, May. 2016 , pp. 1981–1993.

[30]Mohammadimehr, M., Navi, B. R., and Ghorbanpour Arani, A., "Free vibration of viscoelastic double-bonded polymeric nanocomposite plates reinforced by FG-SWCNTs using MSGT , sinusoidal shear deformation theory and meshless method," Composite Structures, Vol. 131, Nov. 2015, pp. 654-671.

[31]Martone, A., Faiella, G., Antonucci, V., Giordano, M., and Zarrelli, M., "The effect of the aspect ratio of carbon nanotubes on their effective reinforcement modulus in an epoxy matrix," Composite Science and Technology, Vol. 71, No. 8, May 2011, pp. 1117–1123.

[32]Liu, G. R., Meshfree Methods: Moving Beyond the Finite Element Method, Second Edition. 2009.

[33]Reddy, J. N., "Mechanics of Laminated Composite Plates and Sheels." pp. 855, 1997.

[34]Efraim, E. and Eisenberger, M., "Exact vibration analysis of variable thickness thick annular isotropic and FGM plates," Journal of Sound and Vibration, Vol. 299, No. 4–5, Feb. 2007, pp. 720–738.

[35]Belytschko, T., Lu, Y., and Gu, L., "Element-free Galerkin methods," Journal of Numerical Methods in Engineering, Vol. 37, No. April 1993, 1994, pp. 229–256.

[36]Zhu, T. and Atluri, S. N., "A modified collocation method and a penalty formulation for enforcing the essential boundary conditions in the element free Galerkin method," Computational Mechanics, Vol. 21, No. 3, Apr. 1998, pp. 211–222.

[37]Chen, J.-S. , Pan, C., Wu, C.T., and Liu, K. W., "Reproducing kernel particle methods for large deformation analysis of non-linear structures," Computer Methods in Applied Mechanics and Engineering, Vol. 139, No. 1–4, pp. 195–227, Dec. 1996.

[38]Memar Ardestan, M. i, Soltani, B., and Shams, Sh., "Analysis of functionally graded stiffened plates based on FSDT utilizing reproducing kernel particle method," Composite Structures, Vol. 112, Feb. 2014. pp. 231–240.

[39]Lam, K. Y., Wang, C. M., and He, X. Q., "Canonical exact solutions for Levy-plates on two-parameter foundation using Green's functions," Engineering Structures, Vol. 22, No. 4, Apr. 2000, pp. 364–378.